Detection of potential fields source boundaries by Enhanced Horizontal Derivative method

Article *in* Geophysical Prospecting · January 2001

DOI: 10.1046/j.1365-2478.2001.00235.x

CITATIONS
207

READS
782

2 authors:

Maurizio Fedi
University of Naples Federico II
264 PUBLICATIONS **3,213** CITATIONS
SEE PROFILE

Giovanni Florio
University of Naples Federico II
121 PUBLICATIONS **1,541** CITATIONS
SEE PROFILE

Geophysical Prospecting, 2001, **49**, 40–58

Detection of potential fields source boundaries by enhanced horizontal derivative method

M. Fedi and G. Florio

Università 'Federico II' di Napoli, Dipartimento di Geofisica e Vulcanologia, Napoli, Italy

Received July 1999, revision accepted June 2000

ABSTRACT

A high-resolution method to image the horizontal boundaries of gravity and magnetic sources is presented (the enhanced horizontal derivative (EHD) method). The EHD is formed by taking the horizontal derivative of a sum of vertical derivatives of increasing order. The location of EHD maxima is used to outline the source boundaries. While for gravity anomalies the method can be applied immediately, magnetic anomalies should be previously reduced to the pole. We found that working on reduced-to-the-pole magnetic anomalies leads to better results than those obtainable by working on magnetic anomalies in dipolar form, even when the magnetization direction parameters are not well estimated. This is confirmed also for other popular methods used to estimate the horizontal location of potential fields source boundaries.

The EHD method is highly flexible, and different conditions of signal-to-noise ratios and depths-to-source can be treated by an appropriate selection of the terms of the summation. A strategy to perform high-order vertical derivatives is also suggested. This involves both frequency- and space-domain transformations and gives more stable results than the usual Fourier method.

The high resolution of the EHD method is demonstrated on a number of synthetic gravity and magnetic fields due to isolated as well as to interfering deep-seated prismatic sources. The resolving power of this method was tested also by comparing the results with those obtained by another high-resolution method based on the analytic signal. The success of the EHD method in the definition of the source boundary is due to the fact that it conveys efficiently all the different boundary information contained in any single term of the sum.

Application to a magnetic data set of a volcanic area in southern Italy helped to define the probable boundaries of a calderic collapse, marked by a number of magmatic intrusions. Previous interpretations of gravity and magnetic fields suggested a subcircular shape for this caldera, the boundaries of which are imaged with better detail using the EHD method.

INTRODUCTION

The horizontal location of the boundaries of gravity and magnetic anomaly sources is a commonly requested task in potential field interpretation. However, the location of the horizontal boundaries of potential field sources is not straightforward, because of the intrinsic loss of resolution of the anomaly shape with respect to the shape of their sources. Knowledge of the locations of the horizontal boundaries of gravity and magnetic sources can be important when investigating the structural setting of a region as well as

Paper presented at the 61st EAGE Conference – Geophysical Division, Helsinki, Finland, June 1998.

for environmental and engineering applications and this information could be included as a constraint in 2D and 3D modelling. Boundary analysis of gridded gravity or magnetic anomalies is at present accomplished using a number of methods involving directional derivatives of different orders. Vertical derivatives have been used for many years to enhance the measured gravity field (Evjen 1936). A well-known method of locating source boundaries is to consider the zero contour of the second vertical derivative of gravity or reduced-to-the-pole magnetic fields. However, as is well known (e.g. Thurston and Smith 1997), the boundaries estimated by this technique are systematically shifted from the true position even for vertical-sided sources, and application of this method produces fairly complicated results in multisource cases. For these reasons, in recent years this method has lost popularity in favour of methods enabling the generation of maps displaying boundaries more clearly and precisely. Cordell and Grauch (1985) showed that the maxima of the horizontal derivative of gravity or pseudo-gravity anomalies are located above abrupt changes of density or magnetization. This technique, coupled with an automated method to locate maxima (Blakely and Simpson 1986), proved to be an effective tool for the boundary analysis. Some authors (Nabighian 1984; Roest, Verhoef and Pilkington 1992) showed that the amplitude of the analytic signal has useful properties, presenting its maxima directly over vertical and abrupt magnetization contrasts. Its most interesting characteristic is the relative insensitivity to the magnetization direction. Another method, based on Euler's equation (Thompson 1982; Reid *et al*. 1990), is often used to determine both boundaries and depths-to-source of magnetic or gravity anomalies. Results of this method are dependent to a limited extent on the magnetization direction, but it is necessary to input a parameter, the so-called 'structural index', depending on the unknown geometrical characteristics of the source and of its depth. More recently, the analytic-signal method was generalized to higher-order derivatives to increase the resolving power of this technique (Hsu, Sibuet and Shyu 1996; Hsu, Coppens and Shyu 1998). These authors suggested the computation of the 'enhanced' analytic signal starting from the second vertical derivative of the first derivatives along the *x*-, *y*- and *z*-directions of the magnetic field, and showed also some formulae to compute the depth-to-source by means of amplitude ratios between analytic signals of different orders.

The most appealing characteristic of all these methods is that it is possible to obtain quantitative results on gridded data in a semi-automatic way and with only a few assumptions. One of the main limitations to making a good estimate of the position of a boundary of a source are interference effects caused by nearby sources, especially when they are deep-seated. The enhanced horizontal derivative (EHD) method is presented here as a high-resolution boundary-analysis technique.

THE EHD METHOD

Definition

An n-dimensional real function $f(x_1, x_2, x_3, \ldots, x_n)$ such that all the derivatives of order m exist and are continuous in the interval $a_i < x_i < b_i\ (i = 1, 2, \ldots, n)$ can be approximated by $m + 1$ terms of a multiple Taylor expansion (Korn and Korn 1968). When $n = 3$, it can be written:

$$f(x_1, x_2, x_3) = f(a_1, a_2, a_3) + \sum_{i=1}^{3} \left[\frac{\partial f}{\partial x_i}\right]_{a_1,a_2,a_3} (x_i - a_i) + \frac{1}{2!}\sum_{i=1}^{3}\sum_{j=1}^{3} \left[\frac{\partial^2 f}{\partial x_i, \partial x_j}\right]_{a_1,a_2,a_3} (x_i - a_i)(x_j - a_j) + \ldots.$$

Considering a potential field measured on a plane $z = z_0$ in the harmonic region, a downward continuation operator can be written as a Taylor series expansion of only the terms related to the vertical axis, because all terms related to the horizontal axes are zero. Putting $x = x_1$, $y = x_2$ and $z = x_3$, we find at any arbitrary (x, y) horizontal location,

$$f(x, y, z) = f(x, y, z_0) + \left[\frac{\partial f}{\partial z}\right]_{z_0} (z - z_0) + \frac{1}{2!}\left[\frac{\partial^2 f}{\partial z^2}\right]_{z_0} (z - z_0)^2 + \ldots + \frac{1}{m!}\left[\frac{\partial^m f}{\partial z^m}\right]_{z_0} (z - z_0)^m. \quad (1)$$

Downward continuation of potential fields has been used to enhance the resolution of potential fields, but it is an unstable transformation and the depth-to-source limits the maximum depth of continuation. Let us now consider a discrete nx^*ny data set and a downward continuation of one grid cell (Δs). On that plane, we have

$$f(x, y, z_0 + \Delta s) = f(x, y, z_0) + f^{(1)}(x, y, z_0)\Delta s + \frac{1}{2!}f^{(2)}(x, y, z_0)\Delta s^2 + \ldots + \frac{1}{m!}f^{(m)}(x, y, z_0)\Delta s^m, \quad (2)$$

where $x = \{\Delta s, \ldots, nx^*\Delta s\}$, $y = \{\Delta s, \ldots, ny^*\Delta s\}$ and $f^{(m)}$ is the discrete mth vertical derivative of f having the physical

Table 1 Geometric and density/magnetization parameters of the synthetic models studied

Model	D.E.	I.E.	D.M./RtP	I.M./RtP	Length	Width	Z_t	Z_b	d/M	Fig.
Isolated gravity	–	–	–	–	13	13	6	10	1.0	5, 6, 7
Isolated magnetic 1	0	60	0/0	60/60	13	13	2	10	1.0	1
Isolated magnetic 2	0	60	0/0	60/60	13	13	0.5	3	1.0	2
Isolated magnetic 3	0	60	0/0	60/60	13	13	6	10	1.0	8
Isolated magnetic 4	0	60	40/0	40/60	13	13	6	10	1.0	3, 9
Isolated magnetic 5	0	60	0/0	60/60	12	12	6	80	1.0	15
Interfering M sources:										
2A	0	60	−20/0	40/60	110	5	4	10	1.0	10
2B	0	60	0/0	60/60	10	5	2	10	0.6	
2C	0	60	40/0	60/60	10	5	4	10	0.8	

D.E., I.E. = Declination, Inclination of the ambient field; D.M./RtP, I.M./RtP = Declination and Inclination of the magnetization/Declination and Inclination assumed to perform reduction to the pole (or pseudogravity transformation); Z_t, Z_b = depth to the top and bottom (km); d/M = model density (g/cm^3) or magnetization (A/m); Fig. = Figure number(s) relevant to test examples in which the model is used.

dimension of f per grid-cell units. For the sake of simplicity, we will consider unscaled derivatives of f, i.e. dimensioned using a unit grid cell. In this case (2) becomes simplified, which is also useful for computational ends, thus

$$f(x,y,z_0+\Delta s) = f(x,y,z_0) + f^{(1)}(x,y,z_0) + \frac{1}{2!}f^{(2)}(x,y,z_0) + \ldots + \frac{1}{m!}f^{(m)}(x,y,z_0). \quad (3)$$

We note that the factorial weights tend to decrease dramatically the importance of the higher-order vertical derivative terms in (3), a determining factor in improving resolution. Abandoning the definition of downward continuation as a Taylor series expansion, we can start instead from (3) to define a new signal ϕ in which the single terms of the summation could be variously weighted, thus replacing the Taylor series factorial weights, so that

$$\phi(x,y,z_0) = f(x,y,z_0) + w_1 f^{(1)}(x,y,z_0) + w_2 f^{(2)}(x,y,z_0) + \ldots + w_m f^{(m)}(x,y,z_0). \quad (4)$$

In the simplest formulation unit weights may be used, so that

$$\phi(x,y,z_0) = f(x,y,z_0) + f^{(1)}(x,y,z_0) + f^{(2)}(x,y,z_0) + \ldots + f^{m}(x,y,z_0). \quad (5)$$

We may now define the EHD as the magnitude of the horizontal derivative of ϕ,

$$EHD(x,y) = \sqrt{\left[\left(\frac{\partial\phi}{\partial x}\right)^2 + \left(\frac{\partial\phi}{\partial y}\right)^2\right]}. \quad (6)$$

As we show below, the EHD may be computed starting from any order derivative of the gravity or magnetic potential. As for the Taylor series (equation (1)), the physical dimensions of ϕ, and consequently of the EHD, will therefore depend on the above choice. Analogously to the horizontal derivative method, boundaries can be outlined by considering the location of the maxima of the EHD function.

An important feature of this method is that the horizontal derivatives of the different terms of the summation contribute differently to the definition of the source boundaries (see section on 'Isolated gravity source' below). The maxima of higher-order terms tend to be located on the source corners, while those of the lower-order derivatives are more useful for defining the main lineaments of the sources.

Equation (5) can be adapted to specific cases of interest, in the sense that it is possible to choose the most appropriate set of terms to be considered in the summation (Figs 1 and 2). Figure 1 shows the plots of several normalized EHD signals obtained using different starting functions in (5) (i.e. pseudogravity anomaly, magnetic field, its first vertical derivative, etc.). EHD signals are plotted as profiles extracted along the S–N direction from maps relating to 3D calculations. The analysed field is a magnetic anomaly, its source being a 2 km deep vertical prism (see Table 1). First of all, a general improvement in resolution has to be noted when considering more than one single term in (5) (compare Fig. 1a with b, c with d, e with f, g with h). It is also clear that the EHD signal computed starting from the pseudogravity anomaly gives the more stable, but less resolved results (Fig. 1b), while the EHD computed starting from the second vertical derivative is characterized by strong secondary maxima that may not allow a precise estimation of the

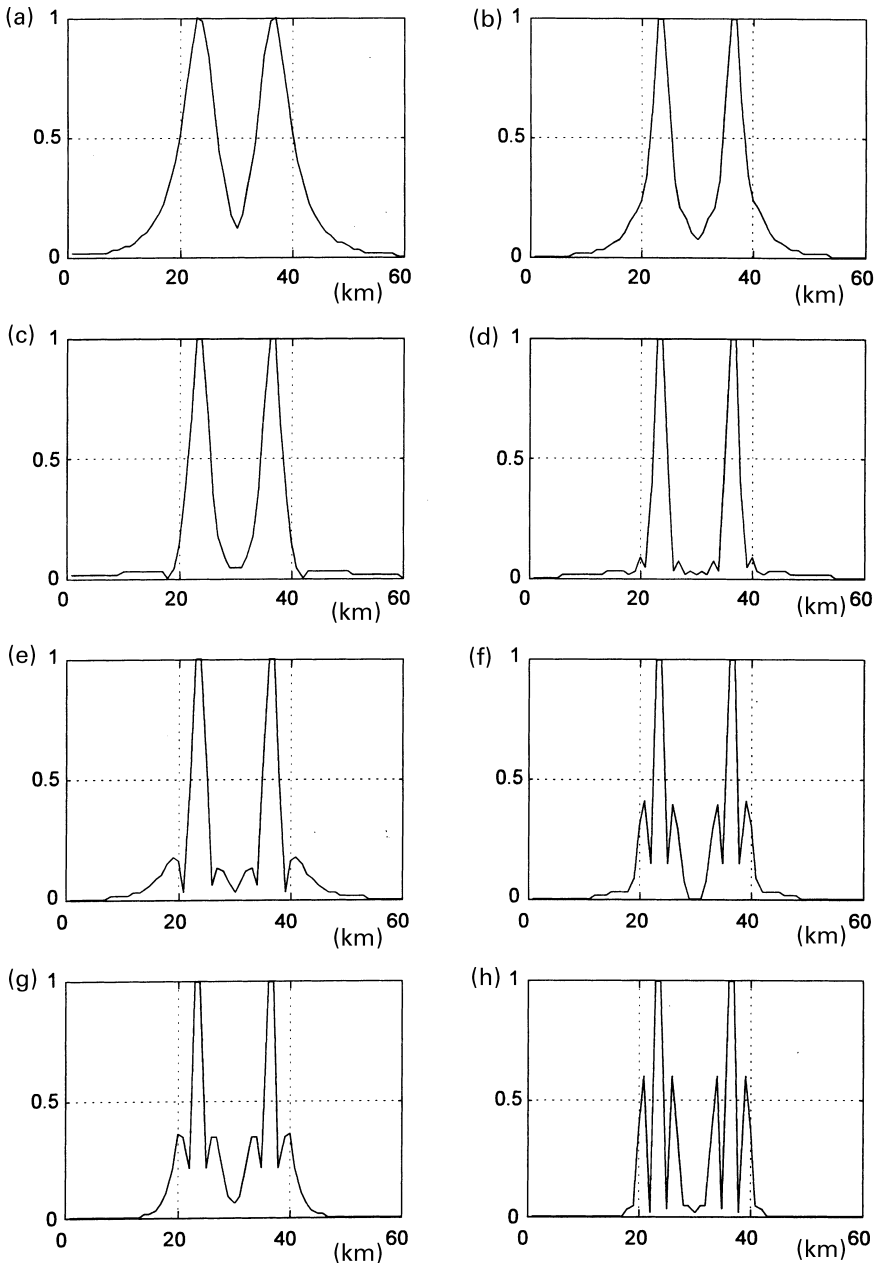

Figure 1 Normalized EHD signals along S–N profiles above a magnetized prism having its top at 2 km depth (see Table 1). (a) ϕ is composed of the pseudogravity field only, (b) its vertical derivatives up to eighth order are included; (c) ϕ is composed of the magnetic field only, (d) its vertical derivatives up to seventh order are included; (e) ϕ is composed of the first vertical derivative of magnetic field only, (f) its vertical derivatives up to sixth order are included; (g) ϕ is composed of the second vertical derivative of magnetic field only, (h) its vertical derivatives up to fifth order are included. The boundaries of the prisms are at $x = 24.5$ km and $x = 37.5$ km.

source boundaries location (Fig. 1h). The EHD signal displaying the best trade-off between resolution and noise amplitude is, in this specific example, that computed starting from the magnetic field and considering terms up to its seventh vertical derivative (Fig. 1d). In this case, in fact, the maxima are very sharp, enabling the horizontal location of the prism to be identified with very good resolution. Only a negligible amount of amplitude noise (spurious maxima) is present.

However, in the study of anomalies with different frequency content, for example generated by the same source as Fig. 1, but located at a different depth, the EHD signal displaying the best trade-off between resolution and noise amplitude may no longer be that computed starting from the magnetic field as in the previous case (Fig. 1). For example, Fig. 2 illustrates the case of a magnetized prism only 0.5 km deep. In this case the best result is obtained by an EHD signal computed starting from a pseudogravity anomaly up to its fourth vertical derivative (Fig. 2b). The EHD signal computed in this way is very sharp and presents the best signal-to-

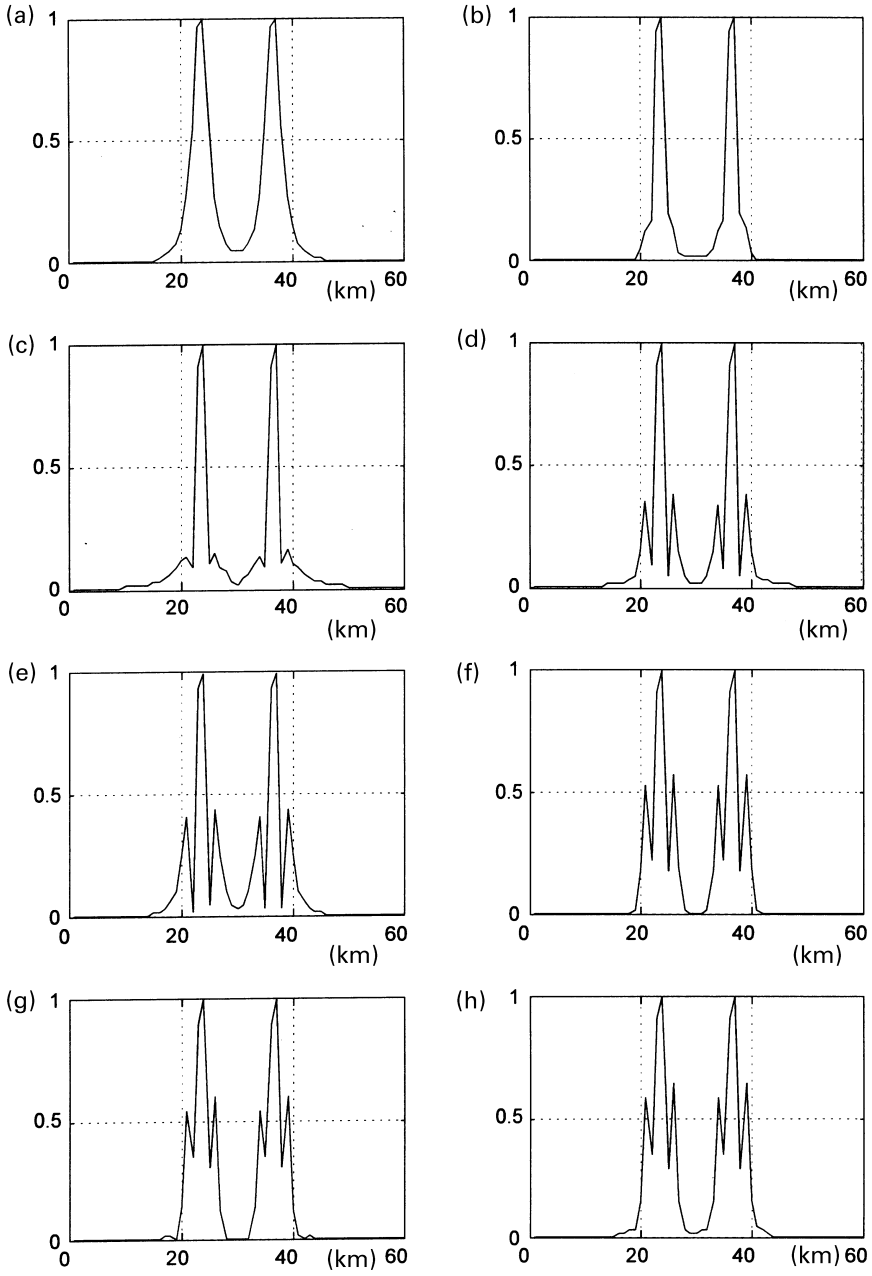

Figure 2 Normalized EHD signals along N–S profiles above a magnetized prism having its top at 0.5 km depth (see Table 1). (a) ϕ is composed of the pseudo-gravity field only, (b) its vertical derivatives up to sixth order are included; (c) ϕ is composed of the magnetic field only, (d) its vertical derivatives up to fifth order are included; (e) ϕ is composed of the first vertical derivative of magnetic field only, (f) its vertical derivatives up to fourth order are included; (g) ϕ is composed of the second vertical derivative of magnetic field only, (h) its vertical derivatives up to third order are included. The boundaries of the prisms are at $x = 24.5$ km and $x = 37.5$ km.

noise ratio with respect to all the signals which can be computed starting from higher-order terms. In fact, even the horizontal derivative of the reduced-to-the-pole magnetic field alone (Fig. 2c) presents maxima not related to the source boundaries, and these spurious maxima are amplified when higher-order terms are added in (5) (Fig. 2d). Starting from the first or the second vertical derivative of the magnetic field leads to signal-to-noise ratios even lower (Fig. 2e–h). Similar conclusions may be obtained in the cases of fields characterized by the presence of a low signal-to-noise ratio at high frequencies.

In the cases of deeper sources, which generate smooth fields, the EHD function should, instead, be computed starting from the first or the second vertical derivative of the measured field. In fact, eliminating the stable low-order terms and considering only the higher-resolution ones may constitute the best choice to enhance the information contained in the field. Note that, for these sources, high

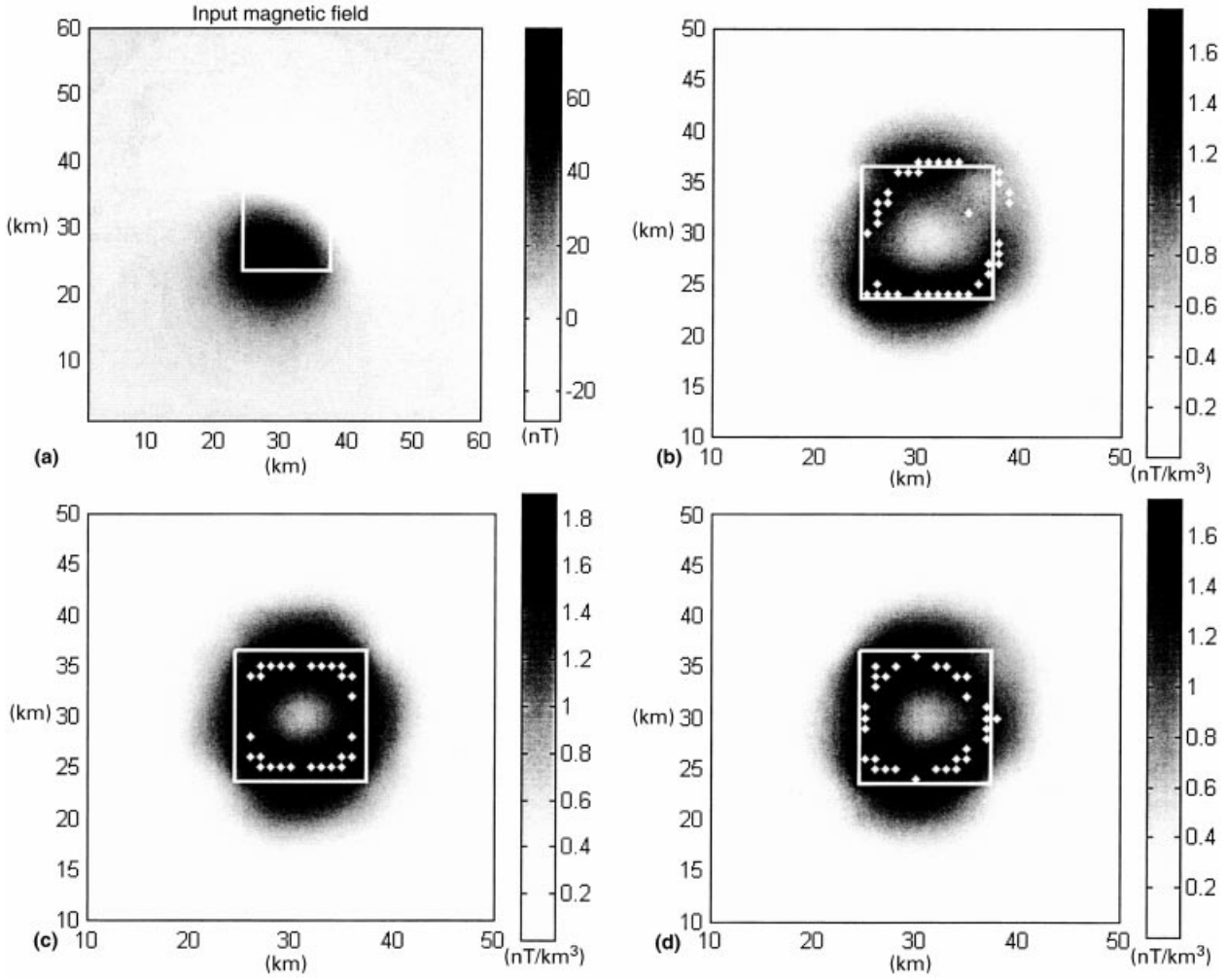

Figure 3 Source boundaries found by means of a second-order enhanced analytic signal (EAS; Hsu *et al*. 1996). (a) Magnetic field generated by a magnetized isolated source (see source parameters list in Table 1). In this and in all the following figures, white dots indicate EAS (or EHD) maxima while the source boundary is outlined with a white line. (b) shows the EAS from the anomaly in its dipolar form (a). An improved boundary is shown in (c), after reduction to the pole (using the correct direction of magnetization). Even when parameters of magnetization are far from the true ones ((d), see Table 1), analysis of reduced-to-the-pole data allows a better boundary to be obtained (compare with (b)).

values of the signal-to-noise ratio are still maintained due to the low high-frequency content of the input field.

Boundary analysis of reduced-to-the-pole magnetic data

While for gravity anomalies the method can be applied directly, magnetic anomalies should be previously reduced to the pole to obtain maxima indicating the source boundaries by the horizontal derivative of $\phi(z)$, analogously to the method of the simple horizontal derivative (Cordell and Grauch 1985). This transformation needs some care, because the source magnetization direction is generally unknown. In recent years several boundary-analysis methods (analytic signal, Euler deconvolution, etc.) were claimed not to depend on the magnetization direction (e.g. Reid *et al*. 1990; Qin 1994). Other authors have instead pointed out that such a dependence indeed exists (e.g. Agarwal and Shaw 1996; Ravat 1996; Linping, Znining and Changli 1997; Linping and Zhining 1998). We found that the analysis of reduced-to-the-pole data improves the definition of boundaries found with these techniques. This is the case also when the parameters of magnetization direction chosen for the reduction to the pole are far from the real ones. In fact, even if the boundary location estimated by such techniques displays a shift from

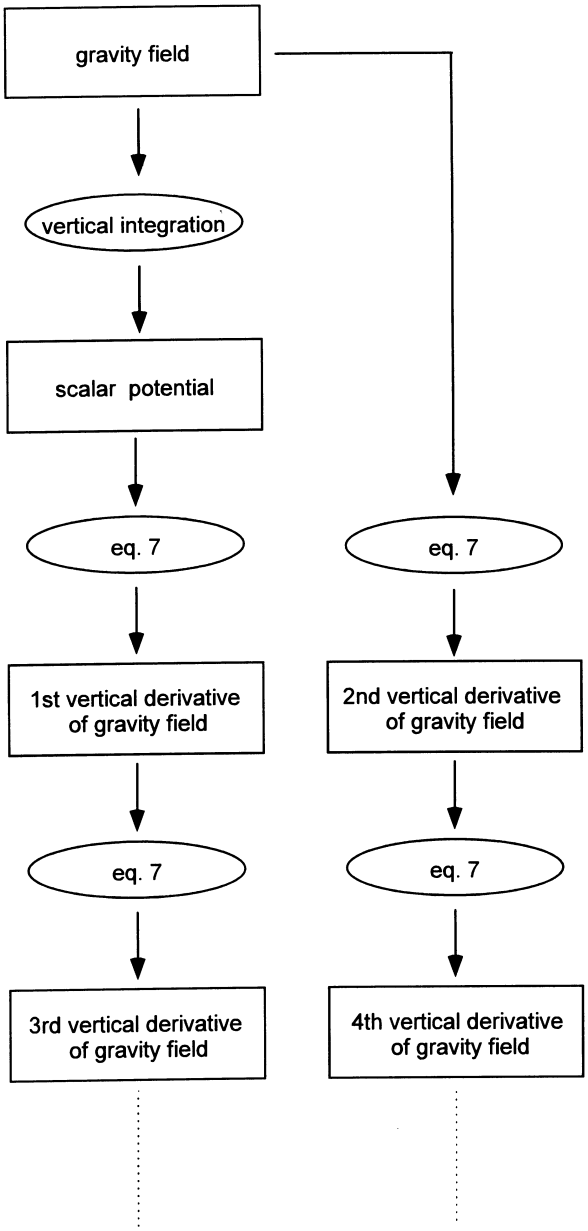

Figure 4 Scheme of the proposed strategy for performing stable high-order vertical derivatives of a gravity (or magnetic) field by using the Laplace equation (7).

the true position, this offset tends to reduce as the order of derivatives used increases. The EHD method also clearly shows this behaviour. In Fig. 3, the boundaries found by means of the second-order enhanced analytic signal (Hsu *et al.* 1996) of magnetic data reduced to the pole with either correct or incorrect magnetization parameters (Fig. 3c and d, respectively; see Table 1 for parameters of magnetization) are compared with those found using magnetic data in dipolar form (Fig. 3b). Results show the advantage of the use of reduced-to-the-pole data.

A strategy to perform stable vertical derivatives

To perform derivatives of high order is a critical operation, because the signal-to-noise ratio can get very low. In order to use the EHD method, both vertical and horizontal derivatives are required. As far as horizontal derivatives of gridded data are concerned, their computation can be accomplished in a rather precise and stable way in the space domain by means of finite-differences relationships (e.g. Cordell and Grauch 1985). The vertical derivative of a potential field is sometimes measured, but is more commonly calculated from measured field values by means of a frequency-domain filter operator (Gunn 1975). However, the use of this technique requires very smooth data because any high-frequency noise will be dramatically enhanced with respect to the signal. We suggest a different strategy to perform vertical derivatives which uses transformations in both the frequency and space domains, giving more stable results than the usual Fourier method. In fact, the first vertical derivative of the gravity or magnetic field could be computed in two steps: (i) integrating the field by using a frequency-domain operator to obtain the scalar gravity potential or the pseudogravity anomaly; (ii) computing the second vertical derivative of the integrated function by means of the sum of its second horizontal derivatives (computed by a finite-differences algorithm), according to the Laplace equation,

$$\frac{\partial^2 f}{\partial z^2} = -\left(\frac{\partial^2 f}{\partial x^2} + \frac{\partial^2 f}{\partial y^2}\right). \tag{7}$$

We call this procedure the integrated second vertical derivative (ISVD). A scheme for implementing the computation of ISVDs is illustrated in Fig. 4.

Thus, the vertical derivatives are computed by combining the use of a smoothing filter (the vertical integration filter) and the finite-differences method, which is much more stable than using Fourier horizontal derivatives operators. This is the reason why this procedure allows a lower degrading of the signal-to-noise ratio than the standard Fourier method, especially when the order of computed derivatives increases (Fig. 5).

As always when using Fourier-domain operators, the frequency-domain transformation step needs a sufficiently large extrapolation of the field to avoid important edge errors.

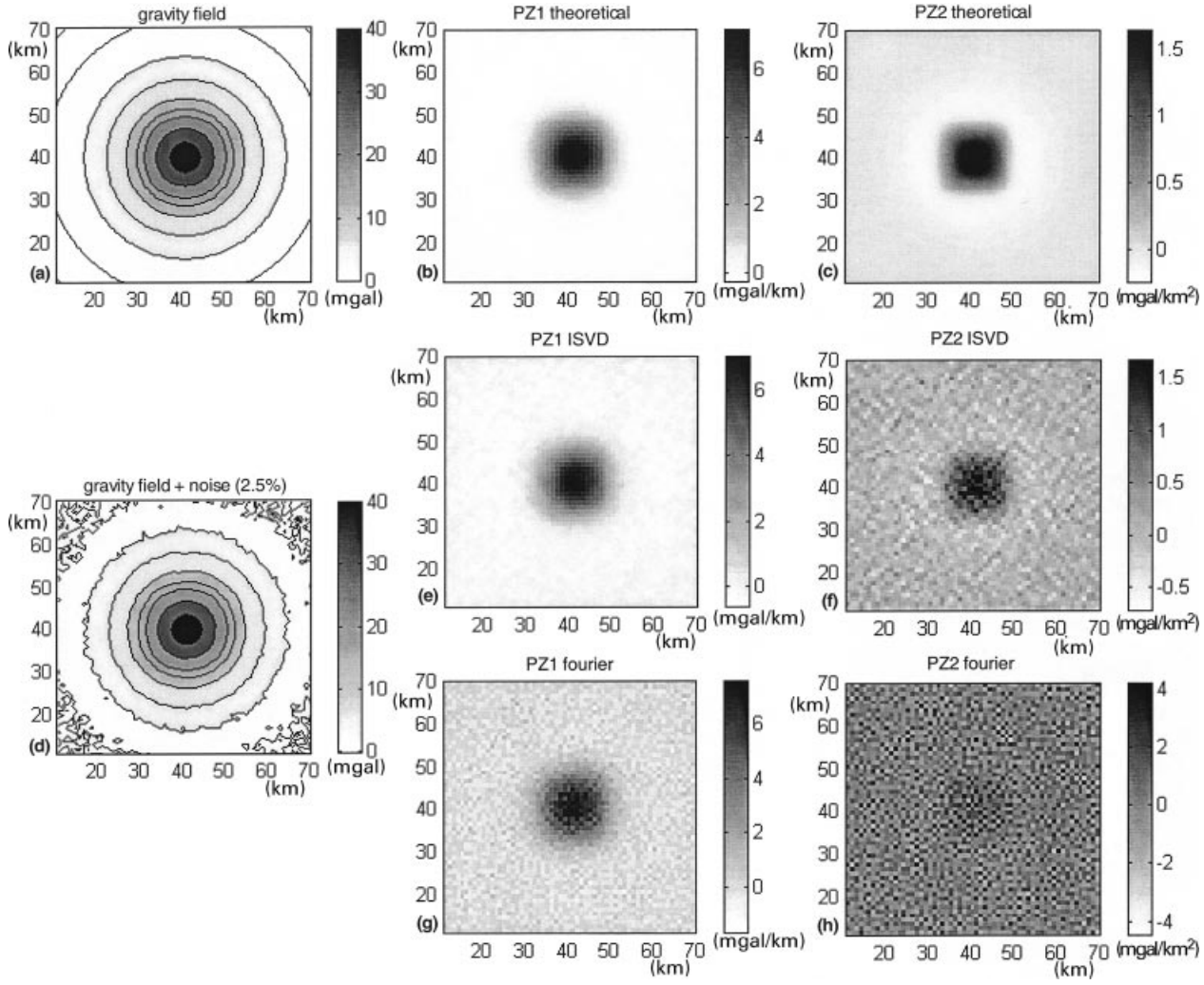

Figure 5 Comparison between the vertical derivative computed by the scheme of Fig. 4 with that computed using the frequency-domain operator. (a) Gravity field of a prismatic source (see Table 1); (b), (c) theoretical first and second vertical derivatives; (d) gravity field of the same source as (a), corrupted with Gaussian noise having an amplitude equal to 2.5% of the original field; (e) first and (f) second ISVD vertical derivatives of the gravity field in (d); (g), (h) frequency-domain vertical derivatives are shown.

SYNTHETIC CASES

In order to test the EHD method we examined various gravity and magnetic anomalies generated by prismatic sources, and compared the boundaries found with those obtainable with another high-resolution method, the so-called 'second-order enhanced analytic signal' (EAS) (Hsu *et al.* 1996):

$$|A_2(x,y)| = \sqrt{\left(\frac{\partial^2 G_x}{\partial z^2}\right)^2 + \left(\frac{\partial^2 G_y}{\partial z^2}\right)^2 + \left(\frac{\partial^2 G_z}{\partial z^2}\right)^2}, \qquad (8)$$

where G_x, G_y and G_z are the first derivatives of the potential field G along the x-, y- and z-directions. We chose to compare the results of our method to those given by the EAS method because in our opinion EAS is at present one of the best techniques to perform high-resolution boundary analysis.

In all the following test examples maxima of both EAS and EHD signals were found by using the method of Blakely and Simpson (1986) with indices 2, 3 and 4 (significance level = 3). For a better evaluation of the resolving power of the EHD method, we tested it on gravity and magnetic fields generated by deep sources, either isolated or interfering.

Isolated gravity source

The gravity anomaly field generated by a deep isolated source

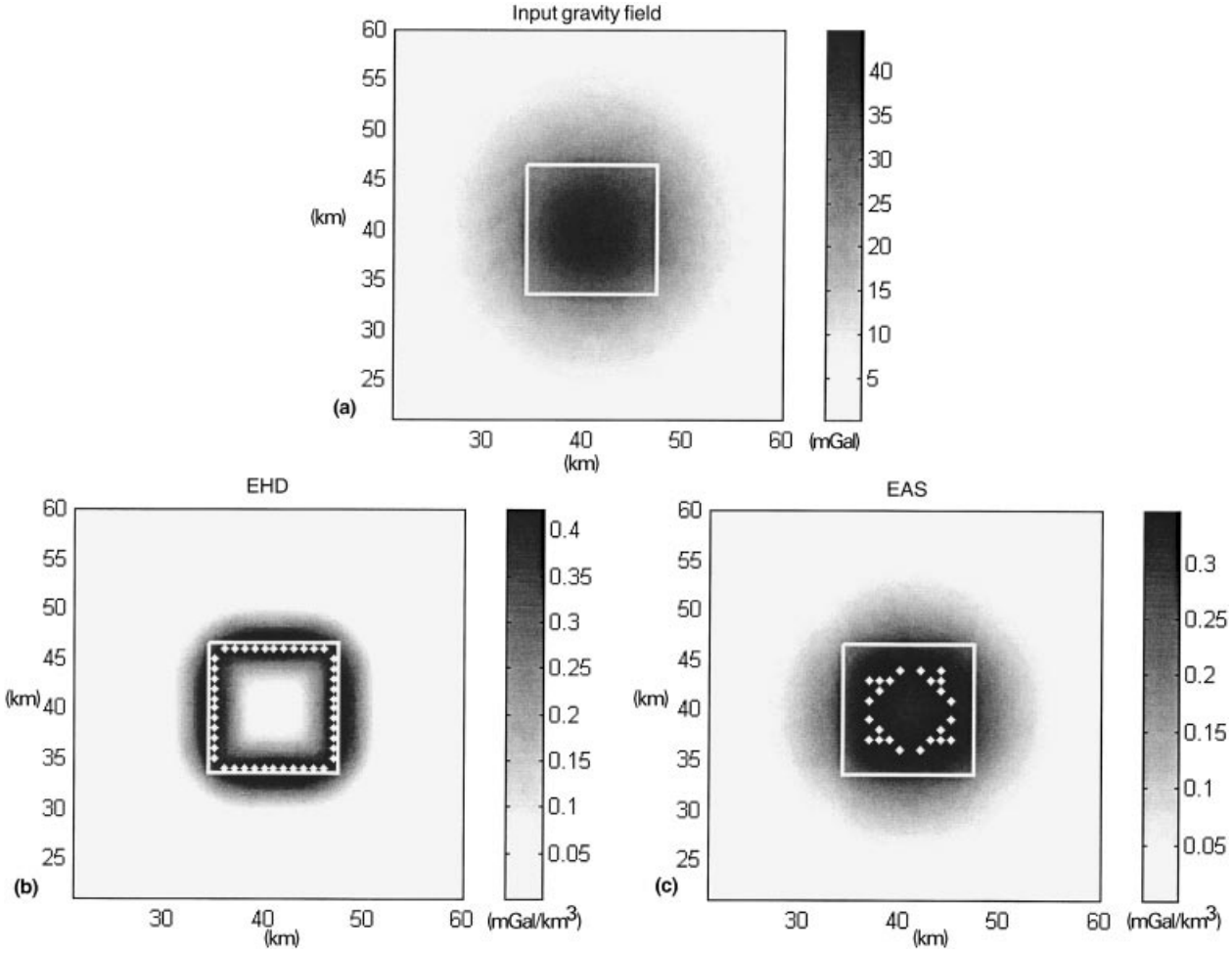

Figure 6 (a) Synthetic gravity field generated by a deep isolated source (Table 1). In (b) and (c) EHD and EAS maxima are compared.

(Table 1) was computed on a grid of 80 × 80 points having 1 km spacing (Fig. 6a). To minimize the errors due to the window size, the field was extrapolated using a maximum-entropy-based extrapolation algorithm (Gibert and Galdeano 1985) to obtain a wider, 180 × 180, grid. The function ϕ (equation (5)) was computed using terms starting from the second vertical derivative of the gravity field up to its fifth vertical derivative. Maxima of the EHD signal allow a very good detection of source boundaries (Fig. 6b). From Fig. 6(c) it is clear that in this case the EAS method does not have enough resolution to outline properly the boundaries of the source. These appear smaller than the true ones (the same effect is shown in fig. 4 of Linping and Zhining 1998). In both cases (EAS and EHD) a high-frequency noise creates low-amplitude spurious maxima. To improve the meaningfulness of the boundary-location estimators, a threshold control on the detection of maxima was applied.

By looking at single horizontal derivatives of various order vertical derivatives (Fig. 7), it is possible to understand better how the EHD method works. In fact the lowest terms of the summation (Fig. 7a,b) have the greatest amplitudes and their inclusion in the summation can counteract the degradation of the signal-to-noise ratio, giving stability to the signal. The horizontal derivatives of the high-order vertical derivatives show a very complicated pattern and tend to display their absolute maxima on the corners of a prismatic source (Fig. 7g–i). When these low-amplitude, high-order terms are included in the summation, they give mainly an increase of resolution at the corners or other details of the source.

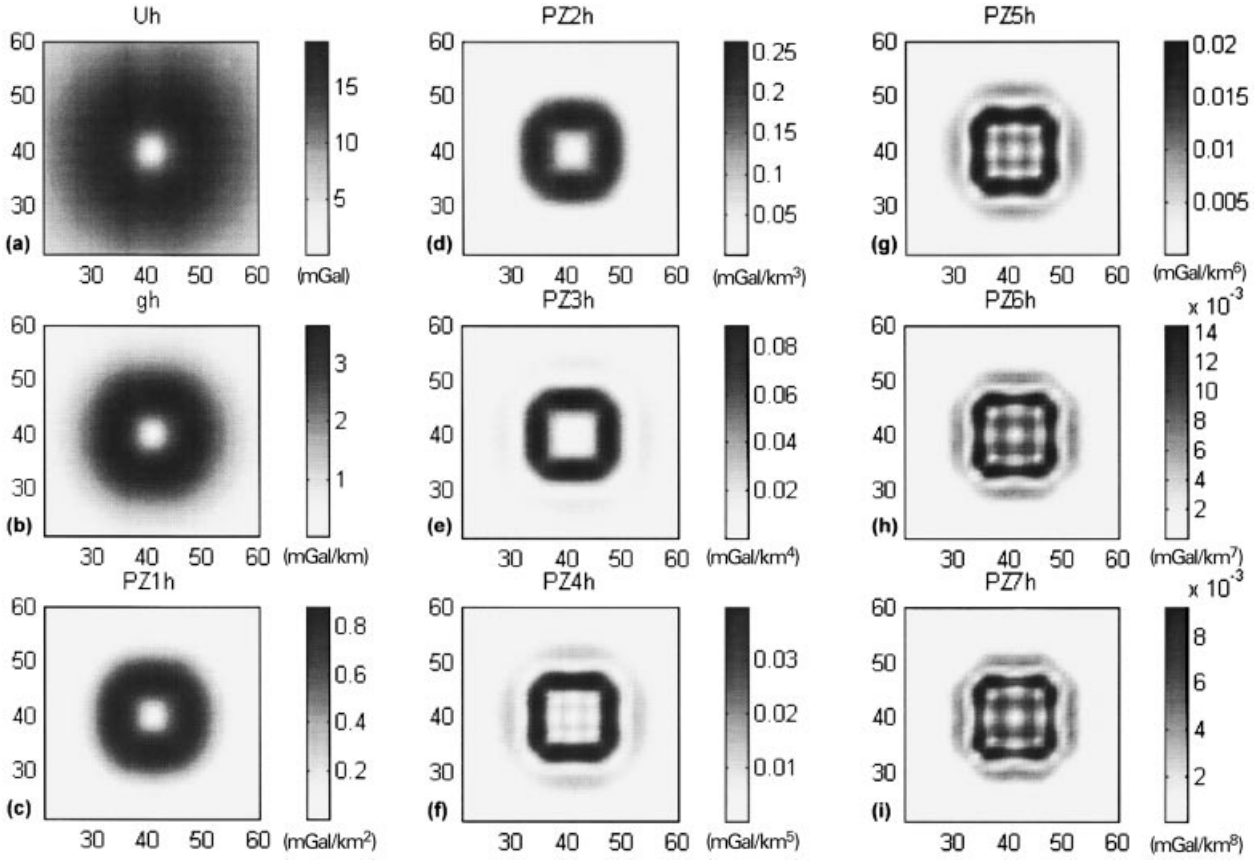

Figure 7 Horizontal derivatives of vertical derivatives of various orders of the same gravity field shown in Fig. 6(a). (a) Horizontal derivative of scalar potential (Uh); (b) horizontal derivative of the gravity field (gh); (c) … (i) horizontal derivative of first vertical derivative of the gravity field (PZ1h) … horizontal derivative of seventh vertical derivative of the gravity field (PZ7h).

Isolated magnetic source

This test considers the same geometric source and grid characteristics as the previous one, now generating a magnetic anomaly (Fig. 8a). Geometric and magnetization parameters are listed in Table 1. The EHD signal was computed starting from the reduced-to-the-pole magnetic anomaly. In this test the parameters of magnetization of the source are known (pure induction case), so that the reduced-to-the-pole anomaly presents no distortions due to an incorrect choice of the magnetization direction. The EHD signal was computed by considering the first vertical derivative of the total field as the lowest-order term of (5), while the highest term was its seventh vertical derivative. The EHD maxima locate precisely the boundaries of the source (Fig. 8b). The results of applying the EAS method to this model test (Fig. 8c) confirm the conclusion that a dependence of analytic-signal methods on the magnetization direction does exist (see section on 'Boundary analysis of reduced-to-the-pole magnetic data' above). In fact the maxima of EAS show an asymmetric pattern due to the dipolar shape of the magnetic anomaly and the sides trending parallel to the magnetization direction (N–S) have the poorest definition.

The computation of the EHD signal was repeated to simulate the most general case, when the reduction to the pole is performed assuming an incorrect direction of magnetization. The difference between the parameters used for the reduction to the pole and the true magnetization direction were 40° on declination and 20° on inclination (see Table 1). Using (5) and starting from the first vertical derivative of the total field up to the seventh vertical derivative, the EHD boundaries still show a good correlation with the true ones (Fig. 9a). The only effects of an inexact reduction to the pole are visible in some distortion of the boundaries and in the presence of an external belt of low-amplitude maxima not related to the true boundaries. Results

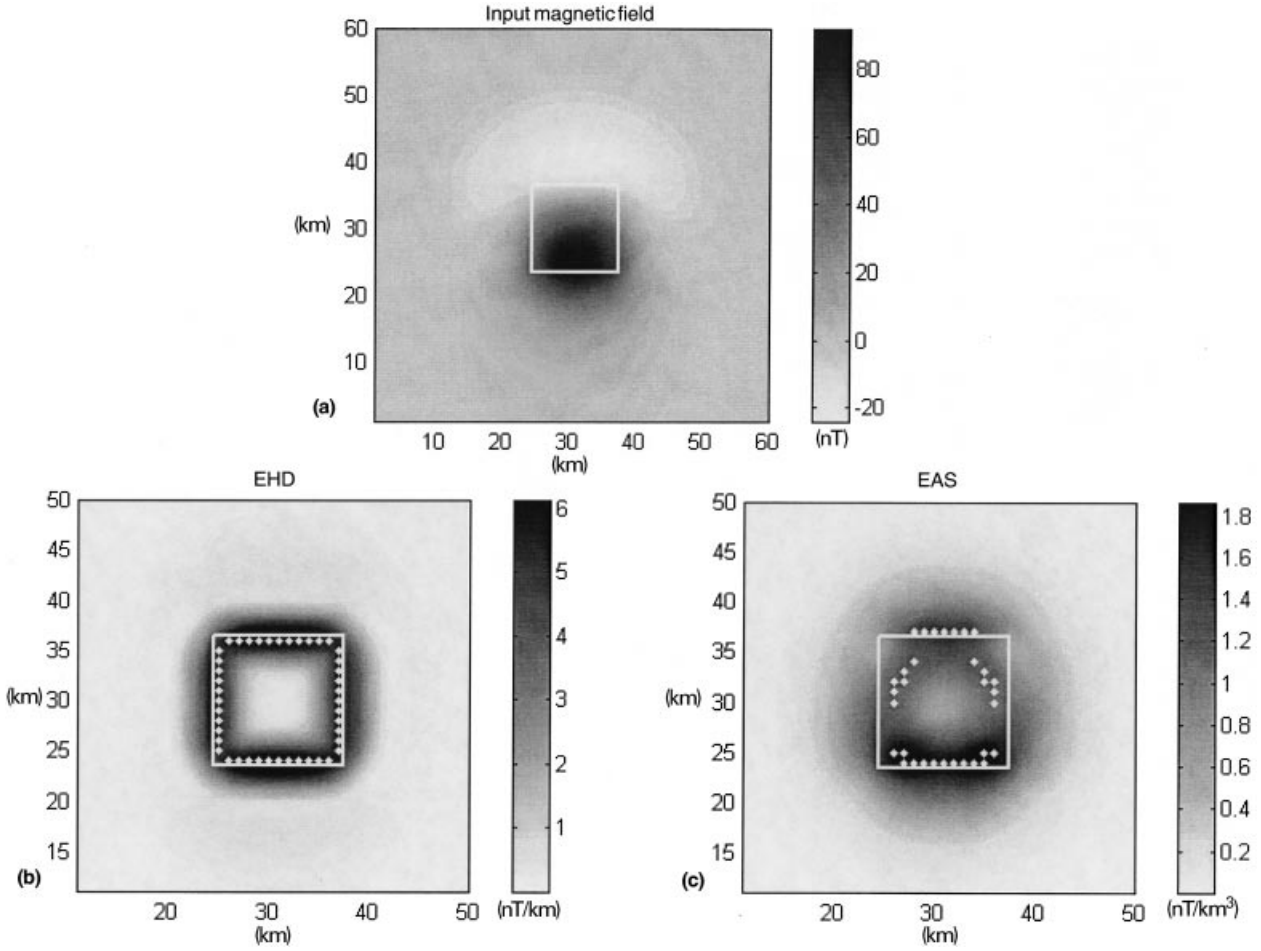

Figure 8 (a) Synthetic magnetic field generated by a deep isolated source (Table 1). (b), (c) EHD and EAS maxima, respectively. For EHD computation the magnetic field was previously reduced to the pole, using the correct direction of magnetization.

improve using (5) starting from the second vertical derivative of the magnetic field up to its seventh vertical derivative, i.e. dropping the lowest-order term, even though the spurious maxima belt now has slightly greater amplitudes (Fig. 9b). Looking at the EAS signal, we note that it has a different shape (Fig. 3b) with respect to the previous example (Fig. 8c), when the source model had a different magnetization direction, again demonstrating a non-negligible dependence on this parameter. The estimated boundaries poorly represent the true ones, particularly along the east side of the prism, corresponding to the position of the magnetic anomaly low (Fig. 3a).

Interfering magnetic sources

Let us now test the performances of the two methods in the more complex case of a magnetic anomaly (Fig. 10a) produced by three close prismatic sources, each one with a different direction of magnetization (see Table 1). The arrangement of the prisms and the grid characteristics are very similar to those adopted in 'model 2' of Hsu *et al.* (1996), but the directions of magnetization and depth to the top of prisms are different. In particular, the prisms are deeper than in the case studied by Hsu *et al.* (1996).

In previous test examples we obtained good results using unit weights (equation (5)). In this case, to resolve well the boundaries of both shallow and deep sources, weights enhancing the role of the high-order derivatives should be used (equation (4)). To this end we generated weights according to $w_m = K^m$, the best results being obtained for $K = 5$.

In Fig. 10(b) the results obtained with the EHD method are

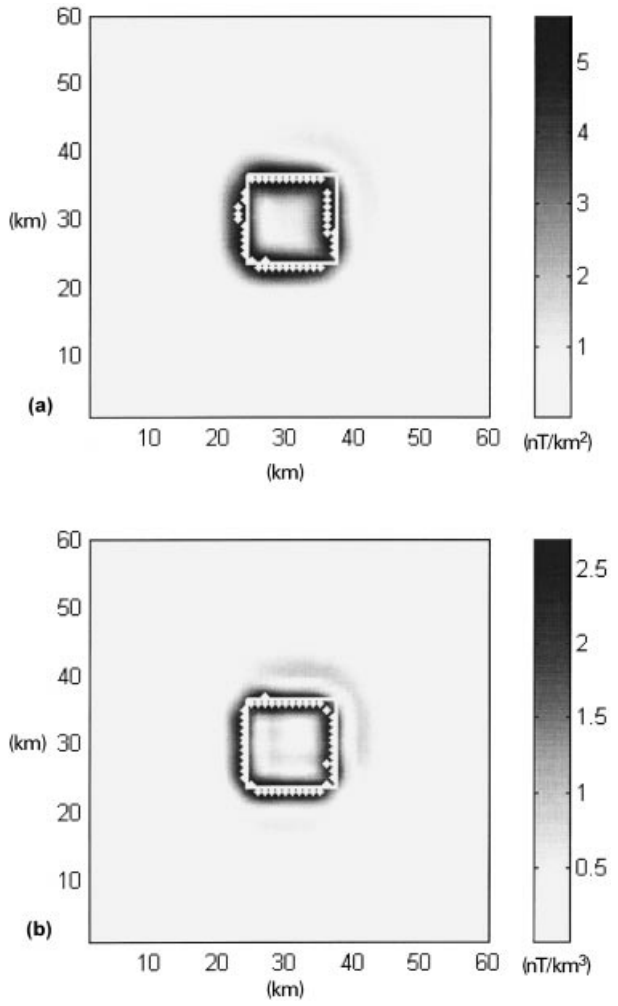

Figure 9 EHD signals computed for the same magnetic field as Fig. 3. In these cases the reduction to the pole was applied assuming an incorrect direction of magnetization (see Table 1). (a) The EHD was computed starting from the first vertical derivative of the magnetic anomaly up to its sixth vertical derivative. (b) To obtain a better resolution, the second vertical derivative of the magnetic anomaly was selected as the starting term.

shown. In this case $\phi(z)$ was computed starting from the magnetic field up to its fourth vertical derivative. Because of the different direction of magnetization, the chosen reduction-to-the-pole parameters correspond to the correct ones only for the prism 2B. The shallowest prism (2B) is outlined satisfactorily, as well as the other two deeper prisms (2A and 2C) which are poorly imaged only along their inner sides, where strong interference effects are present.

Results obtained with the EAS method are shown in Fig. 10(c). The boundaries of the deepest prisms (2A and 2C) are not detectable at all, while those of the shallow one (2B) are imaged with poor resolution.

APPLICATION TO A REAL CASE

The Phlegrean Fields

The Phlegrean Fields are an area of active volcanism located west of the city of Naples, Italy. They are characterized by the presence of a number of small monogenic volcanoes. Their products are mainly pyroclastic rocks and range in composition from trachybasalts to phonolitic alkali-trachytes (e.g. Rosi and Sbrana 1987). Analyses of exploratory geothermal well logs have demonstrated stratigraphic differences at depth between the external and central parts of the Phlegrean Fields (Cassano and La Torre 1987). In fact, in the central part of the volcanic area, the succession appears less rich in lava bodies than in external areas, while greater thicknesses of light pyroclastites occur. This evidence, as well as several volcanological and geophysical studies, indicates the existence of a collapsed structure, interpreted as a caldera.

In the period between 12 000 and 5500 years ago, volcanic activity was concentrated along the edges of this structure (Orsi, De Vita and Di Vito 1996). After a quiescence of about 2000 years, activity developed inside the caldera area as did the last eruption which occurred in 1538 AC, in an area at present densely populated. The definition of the boundaries of the collapsed area may help to outline the areas most exposed to volcanic risk in the case of a new eruption.

Florio *et al.* (1999) have delineated the main structural discontinuities in the Phlegrean Fields area by means of boundary analysis of the gravity and magnetic fields performed by using the simple horizontal derivative method (Cordell and Grauch 1985). The boundaries of the main sources of gravity and magnetic anomalies were found to be substantially consistent, and indicated for the Phlegrean caldera an area less extensive than that defined on the basis of previous geological models. Particularly interesting is the strong correlation found between the dense structures delineated inside the caldera and the positions of the epicentres of recent seismicity.

Aeromagnetic data processing

In 1985 an aeromagnetic survey was carried out in the central area of the Phlegrean Fields. The spacing between the lines of flight was 500 m, the constant flight altitude was 700 m, and the tie lines spacing was 1 km. This aeromagnetic field,

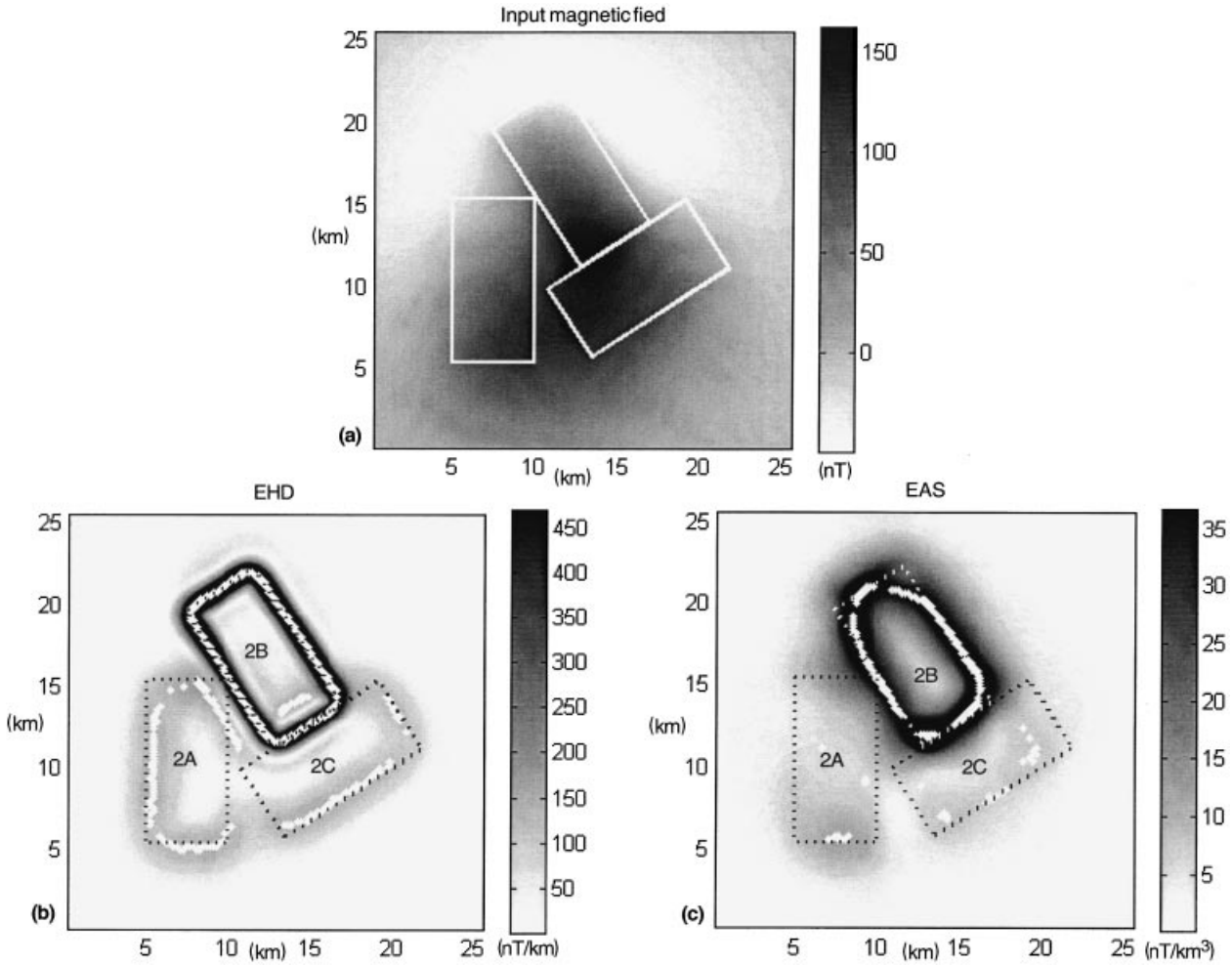

Figure 10 (a) Synthetic magnetic field generated by three close, deep prismatic sources (see Table 1). In (b) and (c) source boundaries obtained by EHD and EAS methods are compared.

reduced to the pole using the local present field direction (declination 0°, inclination 56°; Barberi *et al*. 1991), has three intense highs, while a belt of weak magnetic lows can be seen in the central part of the area (Fig. 11b).

The anomalies were digitized on a regular 0.15 km spacing grid, and a data set consisting of 137 rows and 141 columns was obtained. This data window was then enlarged to 290 rows and 290 columns by means of a maximum-entropy-based extrapolation (Gibert and Galdeano 1985). Two EHD signals were computed starting from the pseudogravity field and considering terms up to the first (Fig. 12a) or second (Fig. 12b) derivative. In both cases (5) was again used with weights according to $w_m = K^m$ with $K = 5$.

In order to compare results, the simple analytic signal (Fig. 12c) and the EAS (Fig. 12d) were also computed. The results demonstrate the better resolution of EHD signals with respect to simple and second-order analytic signals. In fact maxima of analytic signals are not successful in delineating source boundaries and the information they bring is limited to a rough outline of the positions of the anomaly-generating bodies. More meaningful results are instead obtained from the analysis of EHD signals, whose maxima encircle a number of anomaly source bodies, delineating their boundaries.

Interpretation of results

The two maps of EHD signal (Fig. 12a,b) show with different resolution a very interesting arrangement of magnetized bodies. In general it can be noted that most features having strong amplitudes are localized onshore. This can be due

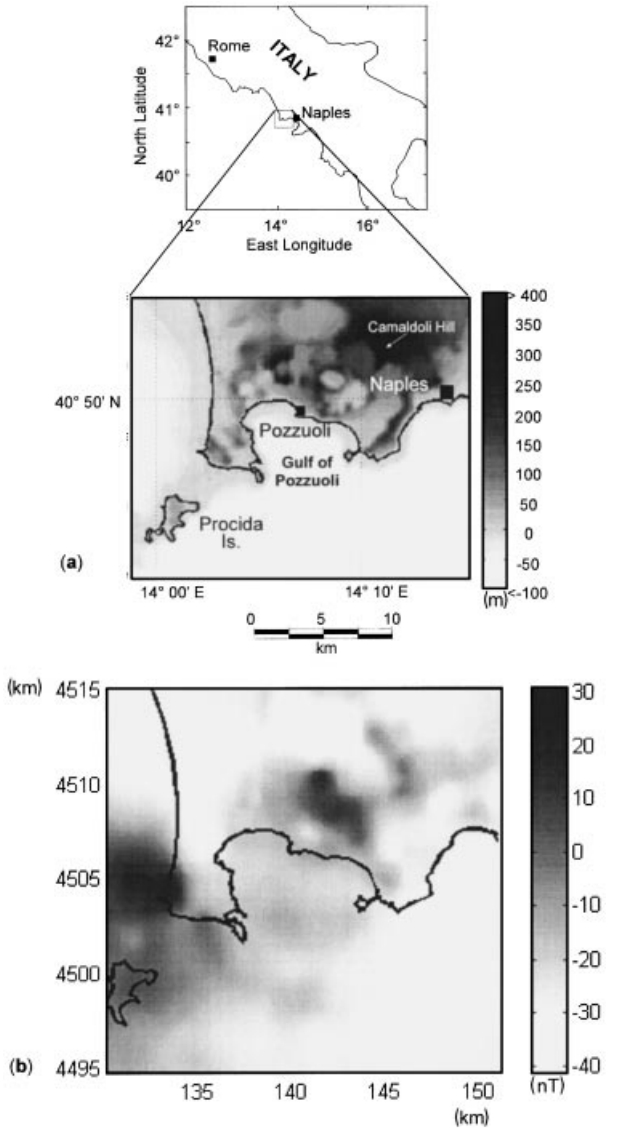

Figure 11 (a) Topographic map of the Phlegrean Fields; (b) reduced-to-the-pole aeromagnetic field of this area.

mainly to the fact that magnetic anomalies were measured at a constant flight altitude (700 m above sea level) and so a certain influence of the topographic relief upon the amplitude of input magnetic anomalies is to be expected. Florio *et al.* (1999) computed the magnetic effect due to topography and noted that the Camaldoli hill (about 450 m above sea level; Fig. 11b) can generate a strong magnetic effect, visible in the aeromagnetic field (and EHD maps) as an NW–SE elongated structure at coordinates 4512N−146E. The distance to the sources offshore is greater than that to the sources onshore (see Fig. 11b), and this is probably the reason why smaller amplitudes of EHD signal are obtained in this area. Despite these differences in resolution and intensity between onshore and offshore, it is possible to identify an alignment of EHD maxima that seems to encircle an area with extremely weak amplitudes of the EHD signal. The ensemble of maxima around this area coincides fairly well with the boundaries of the caldera as identified mainly on the basis of gravity data (Florio *et al.* 1999; Fig. 13). EHD results would suggest delineating the caldera boundaries as linear structures. In this interpretation the pattern of magnetic anomalies would be mainly due to intrusions of magmatic bodies along the fractured caldera boundaries. Other structures, not related to the caldera, are nevertheless present. In particular some anomaly source bodies are identified inside the caldera, in the area that at present shows the greatest activity, at coordinates 4507N−142E. Other identified sources are some isolated bodies on land and north of Procida I., and some linear structures southeast of Procida I. may be caused by a submarine structure.

CONCLUDING REMARKS

The horizontal derivative of a summation of increasing order vertical derivatives of gravity or magnetic fields (loosely referred to as the enhanced horizontal derivative (EHD)) was presented as a new high-resolution method to define the horizontal location of density or magnetization contrasts. The maxima of the EHD function are attained above the boundaries of the potential fields sources. Maps of the EHD maxima (located automatically with the Blakely and Simpson (1986) algorithm) give an immediate and easy-to-read image of the boundaries of the gravity or magnetic sources.

The key to the method is that, due to the sum (6), the EHD signal contains all the boundary details present in any single (derivative) term. Therefore, the process allows a boundary to be defined, which is more complete and informative than any single term of the sum.

One of the main characteristics of this boundary-analysis technique is its flexibility. In fact, to get a high-resolution outline of source boundaries and the best signal-to-noise ratio in the computed EHD, the summation (equations (4) and (5)) may start at the scalar potential (pseudogravity anomaly in the magnetic case) or at some other higher-order vertical derivative (measured field, first vertical derivative of the field, etc.), according to the spectral characteristics of the field. Similarly, an appropriate set of weights may also be important in order to obtain a good resolution.

The high resolution of the EHD method was proved in tests

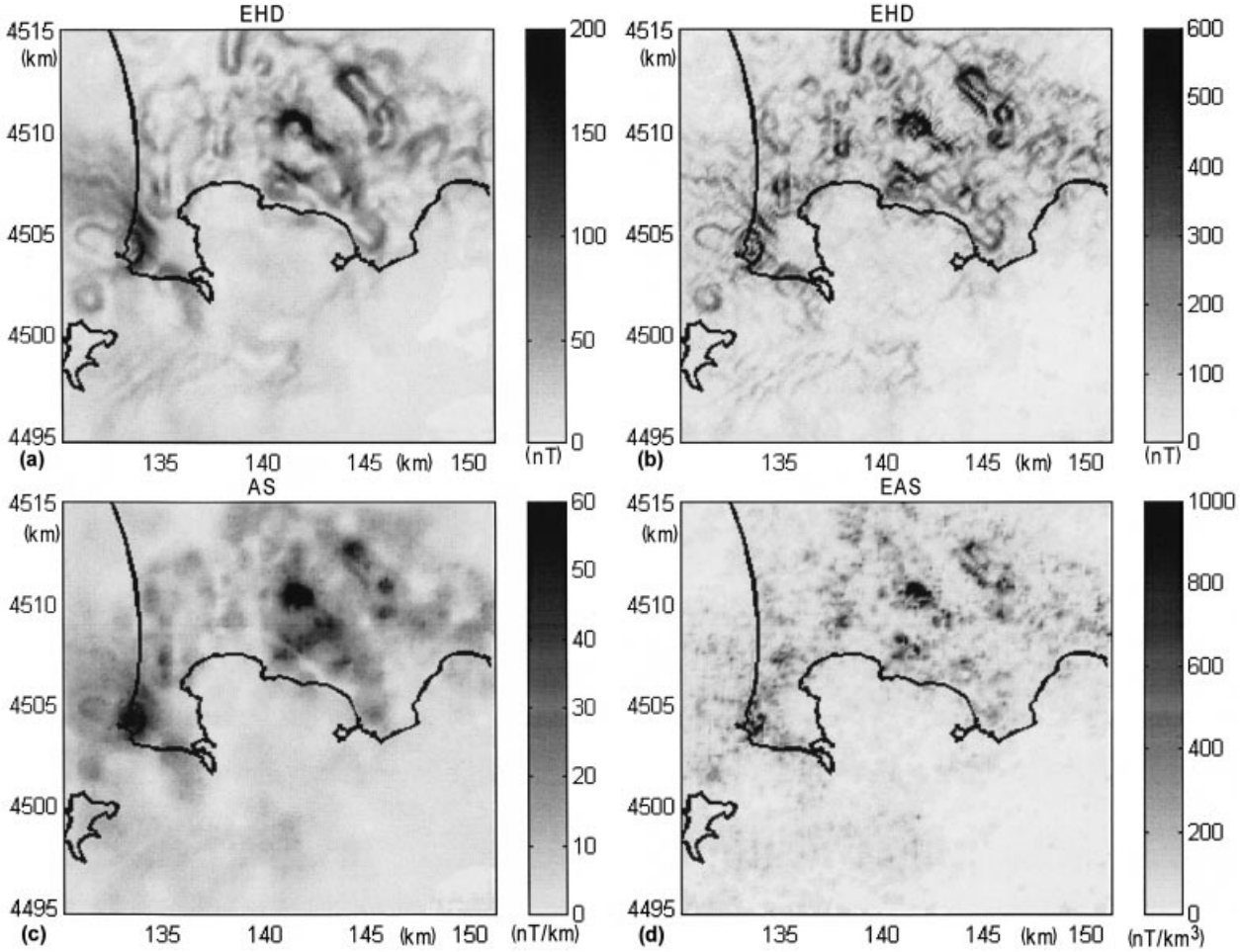

Figure 12 Boundary analysis by EHD and analytic-signal methods of the Phlegrean Fields aeromagnetic data. (a) and (b) show two EHD signals at different resolution in which the lowest-order term was the pseudogravity anomaly and the highest terms were the first and the second vertical derivatives, respectively. (c) and (d) show the simple and the second-order analytic signals.

involving deep sources by comparing these results with those obtained by means of the second-order enhanced analytic signal (Hsu *et al*. 1996).

The method is best applicable to reduced-to-the-pole magnetic data. We showed that even in cases when the input magnetization direction is far from the true one, the boundaries obtained are comparable to or even better than those achieved by other methods using magnetic data in its dipolar form. This result has a general importance because it demonstrates the advantages of working with reduced-to-the-pole magnetic data when using methods which are dependent on the direction of magnetization, such as the analytic-signal method or Euler deconvolution.

The EHD method can involve the use of high-order vertical derivatives, so the importance of performing this transformation in a stable and precise way is critical. To this end a strategy was suggested, involving transformations in both the frequency and space domains, and giving more stable results than the usual Fourier method.

Application to a real aeromagnetic data set of the Phlegrean Fields volcanic area (Italy) demonstrated the efficacy of EHD in practical use, allowing the boundaries of a buried calderic depression to be inferred with better resolution than previous works.

As a future extension of the method, we mention the possibility of computing source-depth estimates along the EHD boundaries. In principle, a depth estimate from each term of the EHD summation could be computed, for example by using an appropriate 'half-width' rule. The EHD depth estimate would then be given by the weighted average of the

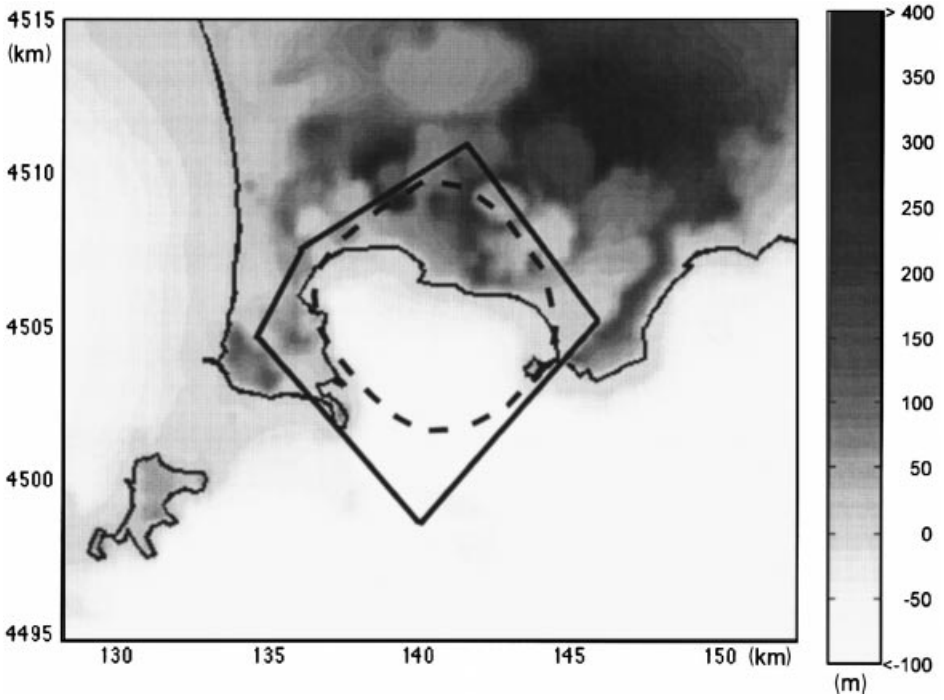

Figure 13 Caldera boundaries interpreted on the basis of analysis of EHD (solid line) compared with those obtained by Florio *et al.* (1999) on the basis of gravity data (dashed line). Grey shading represents the topography.

various estimates relative to the terms of the summation (6), the weights being the same as those used in the computation of EHD. In the Appendix we have applied one of the simplest depth formulae to the various terms of the EHD summation, i.e. the amplitude ratios as proposed by Hsu *et al.* (1996) for the generalized analytic signals of various orders. A test example demonstrates that the average of these depths-to-source computed for the different terms of the EHD summation can actually represent a good depth estimation.

This topic will be fully explored in a future paper. We

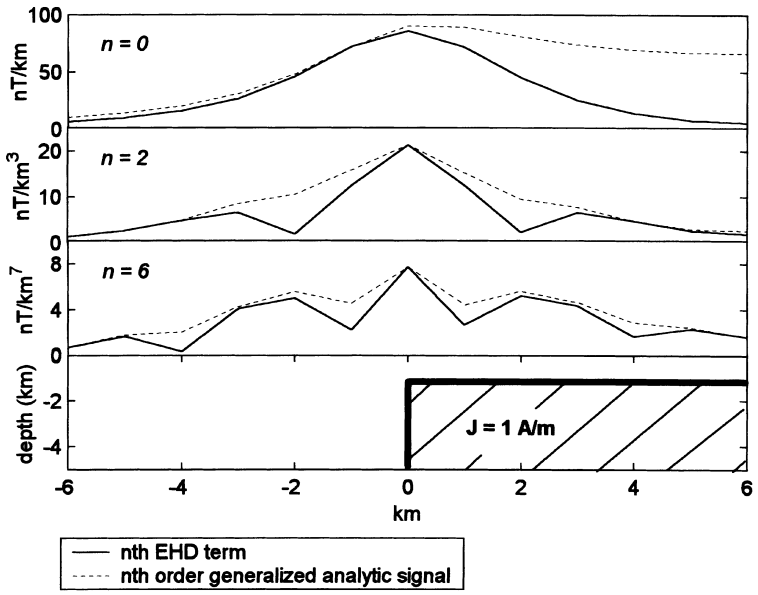

Figure 14 Comparison of EHD and generalized analytic signals for $n = 0$, 2 and 6. The two functions tend to match at maxima, and particularly where a vertical and abrupt source edge occurs.

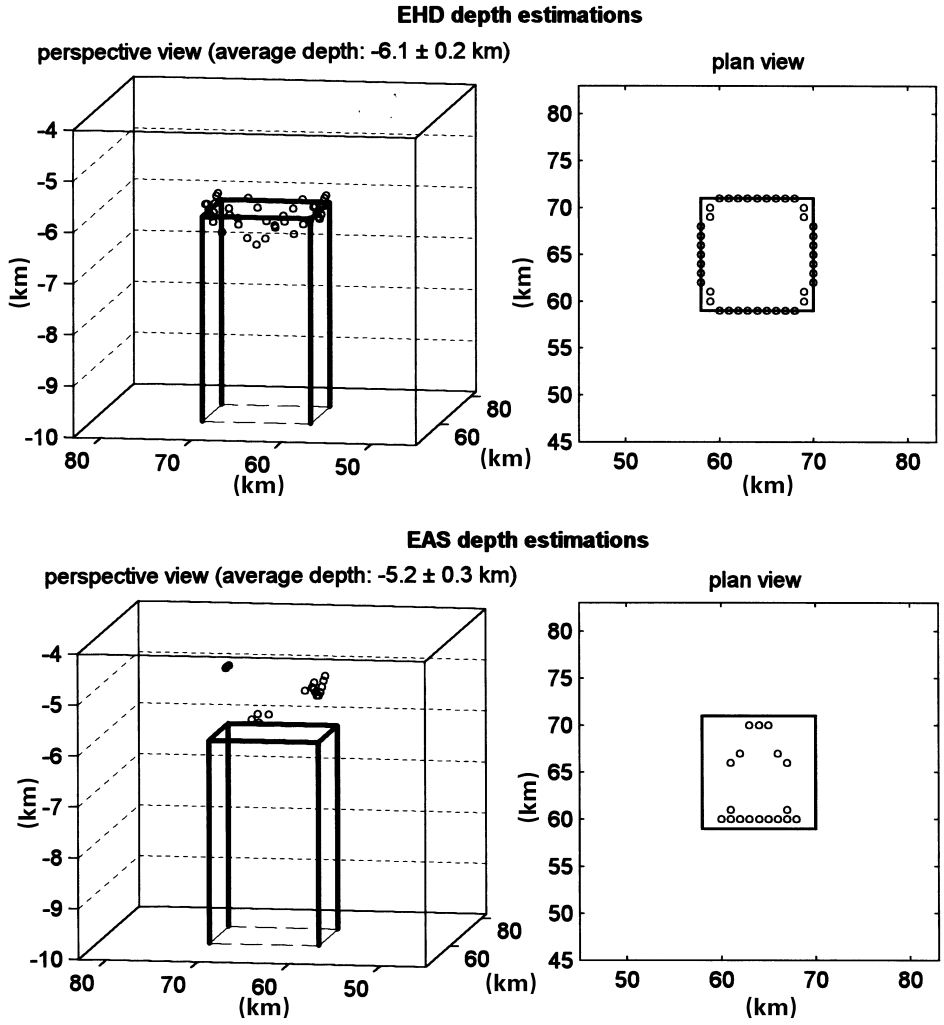

Figure 15 EHD depth and boundary estimates over a prismatic magnetic source buried at a depth of 6 km. For comparison, depth and boundary estimates obtained using the second-order analytic signal are shown.

introduce it here mainly to illustrate the fact that the EHD signal can be useful not only as an enhancement technique of a magnetic or gravity map. In fact, besides the horizontal position of an anomaly source, it can also provide other quantitative estimates of source parameters.

ACKNOWLEDGEMENTS

The authors are indebted to Antonio Rapolla, who has encouraged and critically reviewed the paper. They also thank Bruno Meurers, Alan Reid and an anonymous reviewer for their comments which helped to improve substantially an earlier version of the paper. This research was partially supported by grant MURST 9804330163-006.

REFERENCES

Agarwal B.N.P. and Shaw R.K. 1996. Comment on: 'An analytic signal approach to the interpretation of total field magnetic anomalies' by Shuang Qin. *Geophysical Prospecting* **44**, 911–914.

Barberi F., Cassano E., La Torre P. and Sbrana A. 1991. Structural evolution of Campi Flegrei caldera in light of volcanological and geophysical data. *Journal of Volcanology and Geothermal Research* **48**, 33–49.

Blakely R.J. and Simpson R.W. 1986. Approximating edges of source bodies from magnetic or gravity anomalies. *Geophysics* **51**, 1494–1498.

Cassano E. and La Torre P. 1987. Geophysics. In: *Phlegrean Fields: Quaderni della Ricerca Scientific*, Vol. 114 (eds M. Rosi and A. Sbrana), pp. 103–131. Consiglio Nazionale delle Ricerche.

Cordell L. and Grauch V.J.S. 1985. Mapping basement magnetization zones from aeromagnetic data in the San Juan basin, New

Mexico. In: *The Utility of Regional Gravity and Magnetic Anomaly Maps* (ed. W.J. Hinze), pp. 181–197. Society of Exploration Geophysicists.

Evjen H.M. 1936. The place of the vertical gradient in gravitational interpretations. *Geophysics* **1**, 127–136.

Florio G., Fedi M., Cella F. and Rapolla A. 1999. The Campanian Plain and Phlegrean Fields: structural setting from potential field data. *Journal of Volcanology and Geothermal Research* **91**, 361–379.

Gibert D. and Galdeano A. 1985. A computer program to perform transformations of gravimetric and aeromagnetic surveys. *Computers and Geosciences* **11**, 553–588.

Gunn P.J. 1975. Linear transformations of gravity and magnetic fields. *Geophysical Prospecting* **23**, 300–312.

Hsu S., Coppens D. and Shyu C. 1998. Depth to magnetic source using the generalized analytic signal. *Geophysics* **63**, 1947–1957.

Hsu S., Sibuet J.C. and Shyu C. 1996. High-resolution detection of geologic boundaries from potential field anomalies: an enhanced analytic signal technique. *Geophysics* **61**, 373–386.

Korn G.A. and Korn T.M. 1968. *Mathematical Handbook*. McGraw-Hill Book Co.

Linping H. and Zhining G. 1998. Discussion on 'Magnetic interpretation using the 3-D analytic signal' by W.R. Roest et al. *Geophysics* **63**, 667–670.

Linping H., Zhining G. and Changli Y. 1997. Comment on: 'An analytic signal approach to the interpretation of total field magnetic anomalies' by Shuang Qin. *Geophysical Prospecting* **45**, 879–881.

Nabighian M.N. 1974. Additional comments on the analytic signal of two dimensional magnetic bodies with polygonal cross-section. *Geophysics* **39**, 85–92.

Nabighian M.N. 1984. Toward a three-dimensional automatic interpretation of potential field data via generalized Hilbert transforms: fundamental relations. *Geophysics* **49**, 780–786.

Orsi G., De Vita S. and Di Vito M. 1996. The restless, resurgent Campi Flegrei nested caldera (Italy): constraints on its evolution and configuration. *Journal of Volcanology and Geothermal Research* **74**, 179–214.

Qin S. 1994. An analytic signal approach to the interpretation of total field magnetic anomalies. *Geophysical Prospecting* **42**, 665–675.

Ravat D. 1996. Analysis of the Euler method and its applicability in environmental magnetic investigations. *Journal of Environmental and Engineering Geophysics* **1**, 229–238.

Reid A.B., Allsop J.M., Granser H., Millett A.J. and Somerton I.W. 1990. Magnetic interpretation in three dimensions using Euler deconvolution. *Geophysics* **55**, 80–91.

Roest W.R., Verhoef J. and Pilkington M. 1992. Magnetic interpretation using the 3-D analytic signal. *Geophysics* **57**, 116–125.

Rosi M. and Sbrana A., eds. 1987. Introduction, geological setting of the area, stratigraphy, description of mapped products, petrography, tectonics. In: *Phlegrean Fields: Quaderni della Ricerca Scientifica*, Vol. 114, pp. 9–93. Consiglio Nazionale delle Ricerche.

Thompson D.T. 1982. EULDPH: a new technique for making computer-assisted depth estimates from magnetic data. *Geophysics* **47**, 31–37.

Thurston J.B. and Smith R.S. 1997. Automatic conversion of magnetic data to depth, dip and susceptibility contrast using the SPI method. *Geophysics* **62**, 807–813.

APPENDIX

EHD depth estimations

We tested the application of amplitude ratios as described by Hsu *et al.* (1996) to get depth-to-source estimations along the source boundaries indicated by the EHD. Similarly to the EHD boundary, which is some sort of average of the boundaries related to each term of the sum (6), we may define an EHD depth estimate as the average of the estimations corresponding to each term of the sum. Starting from a previous relationship of Nabighian (1974), Hsu *et al.* (1996) found a simple expression relating the amplitude of the analytic signal A of order n to the depth-to-source d over the edge of a structure with its bottom surface at infinity:

$$|A_n(x,y)| = \sqrt{\left[\left(\frac{\partial f^{(n)}}{\partial x}\right)^2 + \left(\frac{\partial f^{(n)}}{\partial y}\right)^2 + \left(\frac{\partial f^{(n)}}{\partial z}\right)^2\right]} = \frac{n!|\alpha|}{d^n}, \tag{A1}$$

where $f^{(n)}$ denotes the nth vertical derivative of the magnetic field and α is the magnetic field ambient parameter. Hsu *et al.* (1998; equations (6), (7) and (8)) suggested three formulae to estimate depths-to-source, all involving the amplitude ratios of generalized analytic signals of different orders. Let us compare now the horizontal derivative of the reduced-to-the-pole magnetic field, or of its vertical derivative of any order, with the amplitude of generalized analytic signals of the same order (Fig. 14). The two functions tend to match at maxima, and particularly where a vertical and abrupt source edge occurs. The first of these two functions represents simply the various terms of the EHD summation, as the EHD expression (equation (6)) may also be written as

$$EHD(x,y) = \sum_n \sqrt{\left[\left(\frac{\partial f^{(n)}}{\partial x}\right)^2 + \left(\frac{\partial f^{(n)}}{\partial y}\right)^2\right]}.$$

So, over a vertical and abrupt edge of an anomaly source, each EHD term approximates the generalized analytic signal of the corresponding order:

$$EHD_n(x,y) = \sqrt{\left[\left(\frac{\partial f^{(n)}}{\partial x}\right)^2 + \left(\frac{\partial f^{(n)}}{\partial y}\right)^2\right]} \approx A_n(x,y).$$

This implies that we can apply the amplitude ratios proposed by Hsu *et al.* (1998) to the various EHD terms. In other words, we may change the Hsu *et al.* (1998) depth formulae into the following ones, involving the ratios between the

various terms of the EHD signal of different order n at the location of maximum ($EHD_n(0)$):

$$d = \frac{|EHD_n(0)|}{|EHD_{n+1}(0)|}, \tag{A2}$$

$$d = \sqrt{\frac{2|EHD_n(0)|}{|EHD_{n+2}(0)|}}, \tag{A3}$$

where d is the depth-to-source estimate and n is an integer ≥ 0. Note that EHD_0 is the horizontal derivative of the magnetic field, EHD_1 is the horizontal derivative of the first vertical derivative of the magnetic field, etc.

It is now a simple matter to evaluate the depths corresponding to each term of the EHD and to compute their weighted average. In Fig. 15 the EHD depths are shown, obtained for a prismatic source with its top 6 km deep and its bottom at infinity. The EHD was computed using terms from the magnetic field up to its seventh vertical derivative and with unit weights. Each depth estimate along the source boundary represents the average of the estimates computed using (A2) and (A3) with n ranging from 0 to 7. For comparison, we show also the results obtained by using the enhanced analytic signal (Hsu *et al.* 1996) of order 2.